

Information density, structure and entropy in equilibrium and non-equilibrium systems

Mengjie Zu,^{1,2,*} Arunkumar Bupathy,^{3,†} Daan Frenkel,^{2,‡} and Srikanth Sastry^{3,§}

¹*Institute of Physics, Chinese Academy of Sciences,
8 Third South Street, Zhongguancun, Beijing 100190, China.*

²*Department of Chemistry, University of Cambridge, Cambridge, UK.*

³*Theoretical Sciences Unit, Jawaharlal Nehru Centre
for Advanced Scientific Research, Bangalore, India.*

Abstract

During a spontaneous change, a macroscopic physical system will evolve towards a macro-state with more realizations. This observation is at the basis of the Statistical Mechanical version of the Second Law of Thermodynamics, and it provides an interpretation of entropy in terms of probabilities. However, we cannot rely on the statistical-mechanical expressions for entropy in systems that are far from equilibrium. In this paper, we compare various extensions of the definition of entropy, which have been proposed for non-equilibrium systems. It has recently been proposed that measures of information density may serve to quantify entropy in both equilibrium and nonequilibrium systems. We propose a new “bit-wise” method to measure the information density for off-lattice systems. This method does not rely on coarse-graining of the particle coordinates. We then compare different estimates of the system entropy, based on information density and on the structural properties of the system, and check if the various entropies are mutually consistent and, importantly, whether they can detect non-trivial ordering phenomena. We find that, except for simple (one-dimensional) cases, the different methods yield answers that are at best qualitatively similar, and often not even that, although in several cases, different entropy estimates do detect ordering phenomena qualitatively. Our entropy estimates based on bit-wise data compression contain no adjustable scaling factor, and show large quantitative differences with the thermodynamic entropy obtained from equilibrium simulations. Hence, our results suggest that, at present, there is not yet a single, structure-based entropy definition that has general validity for equilibrium and non-equilibrium systems.

* (Equal Contribution) mz410@cam.ac.uk

† (Equal Contribution) bupathy@jncasr.ac.in

‡ df246@cam.ac.uk

§ sastry@jncasr.ac.in

I. INTRODUCTION

The Second Law of Thermodynamics is exceptional among physical laws in that it is usually formulated as an inequality: during a spontaneous change in a closed system, the change in entropy (ΔS) cannot be negative. Since the days of Boltzmann and Zermelo, this property of entropy has given rise to endless debates. However, following Boltzmann, Gibbs and Planck, equilibrium Statistical Mechanics has established a clear link between entropy and probability, and in that framework the second law simply states that a system will spontaneously evolve towards macro-states that have more realizations than the initial macro-state, and are therefore more probable. However, for systems that are intrinsically not in equilibrium - *i.e.*, where neither the initial nor the final macro-state can be described by equilibrium statistical mechanics, it is not *a priori* obvious how to define quantities that have one or more of the properties of entropy.

A simple and robust definition of entropy, dating back to Gibbs, relates S to the probability to find a system (equilibrium or not) in any of its micro-states, *i.e.*,

$$S = -k_B \sum_i p_i \ln p_i, \quad (1)$$

where p_i is the probability of the system being in a micro-state i , and the sum runs over all accessible micro-states.

In equilibrium, computing S is simplified by the fact that the probabilities are known *a priori*. Using numerical free-energy calculation methods [1], the computation of entropy can be extended to more complex cases. Out of equilibrium, the probability of observing a given macro-state becomes protocol dependent and it becomes a challenge to define an entropy that increases during a spontaneous change and provides a measure for the probability of observing a macro-state.

For certain protocols, methods such as basin-volume calculations can be used to compute a Gibbs-style entropy for systems that can be found in a large number of distinct states (e.g. stable packings of granular matter [2–4]). However, such calculations of the “granular entropy” are computationally expensive and, more importantly, may not be applicable to other non-equilibrium situations. It is for this reason that, in the present paper, we will not consider estimates of the entropy based on basin-volume calculations.

A distinct way of computing the entropy of a system from knowledge of its structure,

was developed in the study of fluids at equilibrium: it is based on Kirkwood's factorization of n -body distribution functions [5]. In this formalism, the entropy of an n -body system is expressed as an infinite series: $S = S_{id} + S_2 + S_3 + S_4 + \dots$, where S_{id} is the ideal gas entropy at the given density, and S_n are the contribution due to n -body distribution functions [6–9]. Although the expressions for S_2, S_3, \dots are ensemble invariant [10], and can be used to compute S to arbitrary precision, the numerical difficulties in computing the higher order terms reduce their practical applicability. For our purpose the interesting aspect of an entropy-estimate based on structure alone, is that it can also be used for non-equilibrium systems. However, it is not at all clear that the resulting quantity retains its entropy-like properties out of equilibrium.

Recently, there has been a resurgence of interest in quantifying non-equilibrium entropy in terms of the order or the information content of a variety of physical and biological systems [11–17], using the ideas of algorithmic complexity introduced by Kolmogorov and Chaitin in the context of information theory [18, 19]. The Kolmogorov complexity K is loosely defined as the length of the shortest computer program that can reproduce a given symbolic string. Unlike the Gibbs or Shannon entropy which are statistical measures, K is a measure of complexity or information content which is intrinsic to a given state, and does not require knowledge of the probability distribution of the underlying process. In the context of a many-body system, it is a quantity that can be computed for a single realization of the system.

The interest in K stems from the fact that in the limit of large string length, K is proportional to the Shannon entropy [20, 21]. But given a lack of general principles to compute K , any real complexity analysis has to make use of a universal coding scheme, such as a lossless compression algorithm. The length of the resultant compressed string is then assumed to be the best possible estimate of K , and forms the basis of *computable information density* (CID) measures.

While CID measures have been used in the recent literature to identify order and information content, there is a scarcity of results that connect CID with the thermodynamic entropy. In this paper, we try to answer the question, whether there is a relation between the amount of information contained in an ensemble of micro-states as measured by the CID, and its entropy. Although entropy and order are closely related, it is important to note that statistical-mechanical entropy is actually a measure of the volume of phase space available

to the system. We also emphasize that the different methods discussed here consider only the static structure of the systems for estimating the entropy and do not consider their time evolution, even for the nonequilibrium systems studied. Therefore, the question whether the typical ordering of particles in a given state is related to its entropy must be approached with caution, especially when out-of-equilibrium.

The key point in computing the CID of particle configurations lies in converting them to 1-dimensional strings, which can then be compressed by the appropriate software. This is usually done in the same way as digitizing a photograph, *i.e.*, the particle configurations are digitized onto a regular grid resulting in a set of occupation numbers at each grid point, corresponding to whether a given grid point is occupied by a particle or not. It is then unwrapped into a 1-dimensional string in a way that preserves the spatial patterns or correlations to the extent possible when mapping a higher dimensional system onto a 1D string. Preserving correlations is important as the compression algorithms achieve compression by identifying repeating patterns within the string and replacing them with shorter descriptions. However, the drawback of this kind of discretization is that the results are grid-size dependent. At finer grid sizes, the compression is not very efficient, whereas at coarser grid sizes, there is information loss due to discretization errors. It is clearly less attractive to have an entropy estimate that depends on the choice of the level of discretization.

In this paper, we will consider CID. However, we propose a new method for measuring the information content of particulate systems in continuum space, which does not require the explicit discretization of the co-ordinates as discussed in previous studies. We then investigate the usefulness of CID as a quantitative measure of the entropy. We compare the CID measures with thermodynamic entropy estimates for simple systems in equilibrium, and then extend our studies to non-equilibrium systems of increasing complexity. We identify three classes of systems: (i) systems for which the CID measures show good agreement with other known entropy estimates, (ii) systems where the CID measures identify transitions but where the relationship to entropy is not clear and (iii) systems where the CID measures perform objectively worse than structure based entropy measures.

The rest of the paper is organized as follows. In Sec. II, we present the definitions and the different methods used to quantify the entropy. These include conventional entropy estimates *viz.*, thermodynamic excess entropy and n -body entropy expansions, and compression based information measures. In Sec. III, we present the details of the systems that we have studied

and discuss our numerical results. Finally (Sec. IV), we conclude the paper with a discussion of the implications of our findings.

II. DEFINITIONS AND METHODS

A. Thermodynamic Excess Entropy

Consider a system in thermodynamic equilibrium having a number density $N/V \equiv \rho$ at a temperature T . The excess entropy S_{ex} is defined as the difference between its total entropy S and that of an ideal gas (S_{id}) at the same density and temperature:

$$S_{ex}(\rho, T) = S(\rho, T) - S_{id}(\rho, T). \quad (2)$$

A commonly used technique for measuring the excess entropy in equilibrium simulations is thermodynamic integration [22], where the excess entropy is obtained by integrating the equation of state along a reversible path from the ideal gas state to the target state:

$$\begin{aligned} \frac{S_{ex}(\rho, T)}{Nk_B} &= \frac{U_{ex}(\rho, T) - F_{ex}(\rho, T)}{Nk_B T} \\ &= \frac{U_{ex}(\rho, T)}{Nk_B T} - \int_0^\rho \frac{p_{ex}}{k_B T \rho^2} d\rho, \end{aligned} \quad (3)$$

where $U_{ex} = U - U_{id}$ is the excess internal energy, $F_{ex} = F - F_{id}$ the excess Helmholtz free energy and $p_{ex} = p - p_{id}$ the excess pressure.

B. Pair Correlation Entropy

The excess entropy can be expanded into an infinite series using Kirkwood's factorization [5] of the n -particle distribution function [6–9]:

$$S_{ex} = S_2 + S_3 + \dots, \quad (4)$$

where S_n is the n -body contribution to the entropy. The pair correlation entropy S_2 usually makes the dominant contribution to S_{ex} , and is used as an approximate measure of S_{ex} in studies of liquids and glasses. The ensemble invariant expression of S_2 in terms of the pair correlation function $g(\mathbf{r})$ is given as

$$S_2/Nk_B = -\frac{\rho}{2} \int_0^\infty \{g(\mathbf{r}) \ln g(\mathbf{r}) - [g(\mathbf{r}) - 1]\} d\mathbf{r}. \quad (5)$$

For binary systems with two kinds of particles,

$$S_2 = \sum_{\alpha, \beta} x_\alpha x_\beta S_{2, \alpha\beta}, \quad (6)$$

where x_α is the mole fraction of the α particle, and $S_{2, \alpha\beta}$ is the contribution from the partial pair correlation function $g_{\alpha\beta}(r)$ between α and β particles. In the case of lattice systems, the integral in Eq. 5 is replaced by a sum over the discrete vectors \mathbf{r} .

C. Computable Information Density

Consider a string X of alphabets of length L whose information density we want to find. If $\mathcal{L}(X)$ is the binary code length of the shortest encoding that can reproduce X , then the computable information density (CID) of X is defined as

$$I(X) = \frac{\mathcal{L}(X)}{L} \quad (7)$$

If the string X is compressed using the Lempel-Ziv algorithm (LZ77) [23], the binary code length $\mathcal{L}(X)$ is given as

$$\mathcal{L}(X) \leq C \log_2 C + 2C \log_2(L/C), \quad (8)$$

where C is the number of distinct factors obtained by the LZ77 algorithm from the source sequence X [11]. But in order to compute the information density of an n -particle system, we must first represent it in a form that is suitable for processing by a compression algorithm. More importantly, this representation should preserve the information about the spatial ordering of the particles. We discuss below two such methods.

1. Grid Based CID

In the approach of refs. [11, 12] the CID of an off-lattice n -particle system is computed by first dividing the system into a regular D -dimensional grid with a grid spacing w such that a cell in the grid is occupied by at most one particle. Any grid i which contains the center of a particle (or, for particles with a finite extent, is covered by a particle) is given an occupation number $c_i = 1$. All other grid cells are given $c_i = 0$. In other words, we convert the configuration of particle coordinates into a lattice of occupation numbers. The c_i 's are then encoded into a single string by scanning the grid using a suitable space filling curve

such as the sequential or spiral or Hilbert scan. Here, we use the Hilbert scan which gives the shortest average distance between two successive points along the scan. The Hilbert scan has the added requirement that the number of grid points should be a power of 2. We then compress this string using the Lempel-Ziv algorithm to obtain the CID.

The CID thus computed is an estimate of the total information density or entropy of the system. In order to make comparisons with the thermodynamic excess entropy we need to subtract the corresponding CID of the ideal gas. To do this, we take a random configuration at the same density ρ and calculate its information density I_{id} . The excess information density is defined as

$$I_{ex}(\rho) = I(\rho) - I_{id}(\rho). \quad (9)$$

An important point to note when computing the CID is that the length of the input string for the compression algorithm should be same across different particle densities in order for any data comparison to be valid. This is due to the fact that compression efficiency varies with the input string size. Therefore, for the grid-based CID, we effect changes to particle density ρ by varying the number of particles N and keeping the system size L constant so as to keep the number of grid points constant. We then scale the resultant I by $1/\rho$ so as to estimate the per particle information density. Since the value of the grid-based CID depends on the grid size, any comparison with available thermodynamic entropy data will require the introduction of one scaling parameter, which we determine by least-squares fitting.

2. *Bit-Resolved or Scale-Free CID*

Introducing a grid-based discretization procedure for computing the CID of off-lattice systems, seems arbitrary and less attractive, as the CID can depend on the grid resolution. Below, we introduce a method to convert a configuration of particles into a bit string without any discretization. To this end, we proceed as follows:

1. We use a Hilbert scan to order the particle coordinates. Note that the Hilbert scan has a resolution, but only to the extent that its resolution should be high enough to ensure that the ordering of the particles be unique. Any further increase in resolution makes no difference to the ordering of the particles.
2. Normalize the particle co-ordinates to the range $[0, 1]$, and represent them by 16-bit

integers, except in the case of the 1D gas of hard rods where some information is contained in bits 17-32. The meaning of each bit is easily understood. For example, the leading bit of the x co-ordinate tells whether the particle is in the left (0) or right (1) half of the box. Higher bits correspond to further sub-divisions of the box.

3. Take the value of the j^{th} bit of the particle co-ordinates to form the j^{th} binary string for compression. If X_j^i , Y_j^i and Z_j^i are the j^{th} bit of the co-ordinates of the particle i , then the input string is $X_j^1 Y_j^1 Z_j^1 X_j^2 Y_j^2 Z_j^2 X_j^3 Y_j^3 Z_j^3 \dots X_j^N Y_j^N Z_j^N$.
4. Compress the binary strings using the LZ77 algorithm to estimate the compression density I_j of j^{th} bit.

$$I_j \leq \frac{C_j \log_2 C_j + 2C_j \log_2(N/C_j)}{N}, \quad (10)$$

where C_j is the number of LZ77 factors for the j^{th} string. For all j , the I_j thus computed cannot be larger than I_R , the compression density for a random string of 0s and 1s. However, for higher (i.e. less significant) bits, I_j approaches I_R . We now quantify the total information density as the area between the CID of the random string and that of the target system

$$A = -\frac{D \ln 2}{I_R} \sum_{j=1}^{nbits} (I_R - I_j) \Theta(\Delta_j)$$

$$\Delta_j = \frac{|I_j - \bar{I}_R|}{\sqrt{\bar{I}_R^2 - \bar{I}_R^2}} - 1.0 \quad (11)$$

The conversion factor $D \ln 2 / I_R$ is estimated based on considering the entropy of the ideal gas, which we summarise briefly. Let us consider first the simplest case of the 1D ideal gas. If the particles in the system are confined to the left half of the box, the entropy decrease – compared to the case when the particles are uniformly distributed in the box – is $\ln 2$ per particle. The bit strings representing the particle coordinates for the constrained system have '0's in the first position, with all other bits shifted to the right by one position. The corresponding I_j curve thus shifts to the right by 1 bit, with a resultant increase in the (negative of the) area A by I_R . Thus the conversion factor to obtain the known change in entropy is $\ln 2 / I_R$. In higher dimensions D , considering the scaling of coordinates in each of the D dimensions by $1/2$ we obtain the conversion factor to be $D \ln 2 / I_R$. The CID of any system approaches that of a random string at higher bits, which contains no information

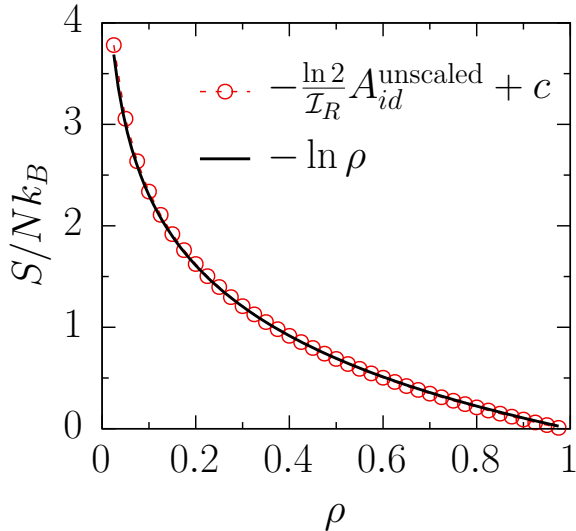


FIG. 1. The total bit-wise information content of 1D ideal gas scaled by $-\ln 2/I_R$, compared with the configurational part of the ideal gas entropy $-\ln \rho$. The constant shift $c = 8.838$.

but is a source of numerical noise. Therefore we only consider the bits where $I < I_R$, as determined by the Heaviside function in the expression above.

We illustrate the validity of the above scaling in Fig. 1, where we have plotted the bit-wise information content of the 1D ideal gas scaled by $-\ln 2/I_R$, as a function of density ρ . The constant shift c is the only fitting parameter involved. Clearly, the scaled value of A_{id} matches well with configurational part of the ideal gas entropy, $-\ln \rho$. For the rest of the results shown, we thus use the expression above for the bit-wise information density.

Note, however, that even an ideal gas A is non zero, because adjacent ideal gas particles tend to have coordinates that differ only a little in the leading few bits. Hence, the meaningful way to quantify the excess CID of an n -particle system is to compute A_{ex} , the *difference* in the area A_{id} for an n -particle ideal gas and the A for n particle system under consideration. Note that the expression for the scale-free excess entropy based on Eq. (11) contains no adjustable parameters and is therefore not subject to fitting.

An alternative (but not equivalent) way to compute the excess CID would be to perform a scale-free compression of the *distances* between successive particles in our Hilbert scan (and subtract the corresponding number for an ideal gas). Below, we discuss both approaches.

III. RESULTS AND DISCUSSION

We first briefly discuss two non-equilibrium model systems that have been studied in [11] using grid-based CID. We include these results only as a validation of our grid-based CID and as a test for the other entropy measures that we use in the remainder of this paper. Note that for the non-equilibrium cases no unambiguous definition for the excess entropy exists. Hence, we compute S_2 as a placeholder for the excess entropy, and compare our CID estimates with it. For equilibrium systems, the difference between the excess entropy and S_2 is often small, making S_2 a credible approximation for S_{ex} . For the binary Lennard-Jones systems described below, available results show that S_2 indeed is a good approximation for S_{ex} [24]. Although inclusion of higher-order correlation entropies (S_3 *etc.*) may result in more accurate values for S_{ex} , we do not expect our results to change qualitatively.

A. The Manna model

The Manna (“sand-pile”) model is defined as follows: Initially, N particles are randomly distributed on a $L \times L$ lattice, with each site i having an occupation number c_i which equals the number of particles at that site. Any site with c_i greater than the threshold z is active. At each step, all the particles on a randomly chosen active site are redistributed randomly over its neighbours. N such steps constitute one cycle. As is well known, this model exhibits a non-equilibrium transition from an absorbing state to an active state as a function of the particle density. For densities below the critical density $\rho_c \approx 0.684$, the number of active sites decay to zero, *i.e.* the system reaches an absorbing state. For $\rho > \rho_c$, the system reaches a steady state with a well-defined fraction of active sites f_a .

To compute the CID, we use the Hilbert scan of the c_i s to generate the input string for data compression. In Fig. 2, we show the pair correlation entropy S_2 , the excess CID I_{ex} , and the excess area of the bit-wise CID A_{ex} for the Manna model on a 512×512 lattice in the steady state (2×10^5 steps), with the threshold for activity $z = 1$. The data has been averaged over 128 samples. Note that the S_2 shown here is *per particle*, not per lattice site. The I_{ex} data has been scaled by a factor of 0.245, to match the S_2 data. We see that both A_{ex} and I_{ex} show a minimum at the critical density ρ_c . Note that, to facilitate comparison with S_2 , we have subtracted the CID corresponding to a random distribution of particles

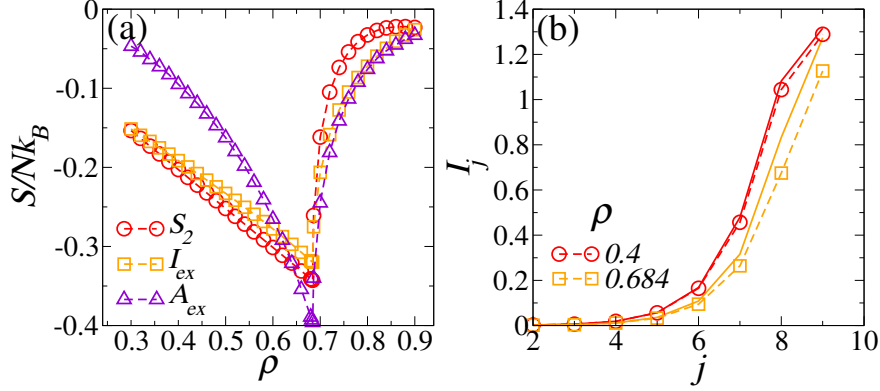


FIG. 2. (a) S_2 , I_{ex} and A_{ex} as a function of ρ , for the Manna model on a 512×512 lattice, in the steady state. The I_{ex} data has been scaled to match S_2 . (b) I_j of the particle co-ordinates vs. j for $\rho = 0.4$ and 0.684 . The solid lines are for the ideal gas at the corresponding densities.

over cells.

In Fig. 2(b), we show I_j of the particle co-ordinates as a function of the bit depth j for two densities $\rho = 0.4$ and 0.684 . The ideal gas reference is also taken on a lattice. The corresponding curves for the ideal gas reference are shown by solid lines. As the points are on a 512^2 lattice, all the bits above $j = 9$ are redundant and carry no information. We find that all three entropy measures are qualitatively similar.

B. The Random Organization Model

The random organization model (ROM) is a continuum analog of the Manna model. It was first introduced to study the reversible state to irreversible state transitions observed in periodically sheared colloidal suspensions [25]. Here we study a simple static variant of the model which is defined as follows: N discs each of diameter d are initially randomly distributed over a $L \times L$ square box. Any overlapping discs are considered active. At each step, *all* active discs are given a small displacement in a random direction. The random displacement imparted to the particle at each step was $d/3$. The state of the system is determined by the packing fraction $\phi = Na_0/A$, where a_0 is the area of a disc and $A = L^2$. System undergoes a dynamical phase transition (from absorbing to active), as ϕ is increased to a critical density $\phi_c \simeq 0.362$.

We control the volume fraction of the system by varying the number of particles in a box

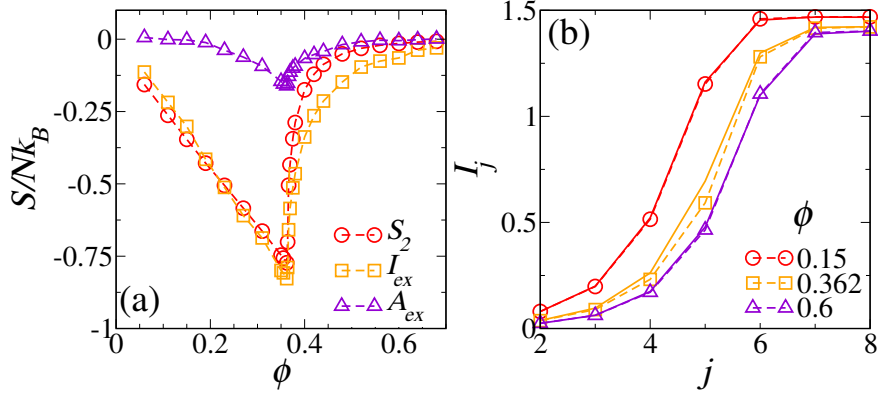


FIG. 3. (a) Various entropy estimates for the random organization model as a function of ϕ . The grid-based CID is scaled to match the S_2 data. The critical packing fraction for the absorbing-to-active state transition is $\phi_c \approx 0.362$. (b) The CID of the particle co-ordinates I_j as a function of bit depth j . The dashed lines correspond to ROM and the ideal gas curves at the corresponding density are shown by solid lines.

with a fixed size $L = 100d$. The configuration has been digitized on a 256×256 grid, leading to a grid width of $\sim 0.4d$. The data that we show correspond to the steady state (after 2×10^5 steps) and has been averaged over 64 samples. Fig. 3 shows the S_2 , the grid based CID I_{ex} and the scale-free CID A_{ex} as a function of ϕ for the ROM. The grid-based CID data is scaled by a factor of 6 to match the S_2 data. Similar to the Manna model, S_2 and I_{ex} show a sharp (cusp-like) minimum at $\phi \approx 0.362$. The excess information A_{ex} computed from the bit-wise CID of particle co-ordinates also shows a cusp-like minimum near the transition, even if it does not show quantitative agreement with the other two entropy measures.

C. 1D Hard Rod Gas

We now consider a number of off-lattice equilibrium systems, for which the entropy is well defined. this allows us to make a quantitative, rather than just qualitative comparison between the entropy of a system and the estimate based on bit-wise data compression. As a first test, we consider a 1-dimensional gas of hard rods as the entropy and radial distribution function of this off-lattice system are known analytically. The equation of state of the hard-rod gas was first derived by Tonks in 1936 [26]. From the analytical equation of state, we then obtain an analytical expression for the excess entropy S_{ex} . For a system with N rods

of size σ in a box of length L , the excess entropy has a simple form:

$$S_{ex}/Nk_B = \ln(1 - \rho\sigma), \quad (12)$$

where $\rho = N/L$ denotes the number density. In addition to the exact excess entropy, we can obtain S_2 by inserting into Eqn. 5 the analytical expression for the pair correlation function:

$$g(r) = \sum_{n=1}^{\infty} \frac{\Theta(r-n)}{1-\rho\sigma} \left(\frac{\rho\sigma}{1-\rho\sigma}(r-n) \right)^{n-1} \times \frac{1}{(n-1)!} \exp \left(-\frac{\rho\sigma}{1-\rho\sigma}(r-n) \right), \quad (13)$$

where Θ is the Heaviside step function and r is measured in units of σ .

For computing the CID, we generate the configurations through Monte Carlo sampling as follows. The system is initialized in a state, with all N rods at a separation of $1/\rho$ along the length L of the box. We then carry out standard Monte Carlo equilibration for 10^5 Monte Carlo steps (MCS) (one MCS equals N single-particle trial moves). The equilibrium properties were then sampled during the subsequent 10^5 MCS, at intervals of 100 MCS, giving a total of 10^3 samples. We perform density changes by varying N and keeping $L = 10^5\sigma$.

In Fig. 4(a), we show S_2 and S_{ex} vs. ρ for the 1D hard rods. The S_2 values are calculated from $g(r)$ obtained from numerical simulations, and have been verified to match with the values computed using the analytical expression of $g(r)$ given in Eq.(13). For densities $\rho \lesssim 0.82$, S_2 underestimates S_{ex} , whereas above it overestimates S_{ex} . This is also generally found to be the case for simple liquids where, for densities below (above) the freezing point S_2 underestimates (overestimates) S_{ex} . We now turn our attention to the various compression-based information density estimates. As discussed in the previous section, we have scaled the CID to obtain an optimal match with the S_{ex} data. Fig. 4(b) shows the grid-based CID measures. The two data sets correspond to the two different discretization procedures (point vs. extended particles) used to convert the particle co-ordinates into a grid of occupation numbers (see Sec. II A.1). A grid spacing of $w = 0.1\sigma$ was used for the discretization of the simulation box. We find that the point representation matches well with the S_{ex} data except at high densities. Taking the finite extent of the rods into account, yields a worse CID estimate of S_{ex} . For the point representation, a grid size of $\approx \sigma/10$ gives the best results. Smaller grid spacing leads to lesser agreement with the excess entropy data (see Fig. 4(c)).

Next, we show the bit-wise information density of the particle co-ordinates and the inter-particle distances as a function of the bit index j in Fig. 4(d) and (e), respectively. The

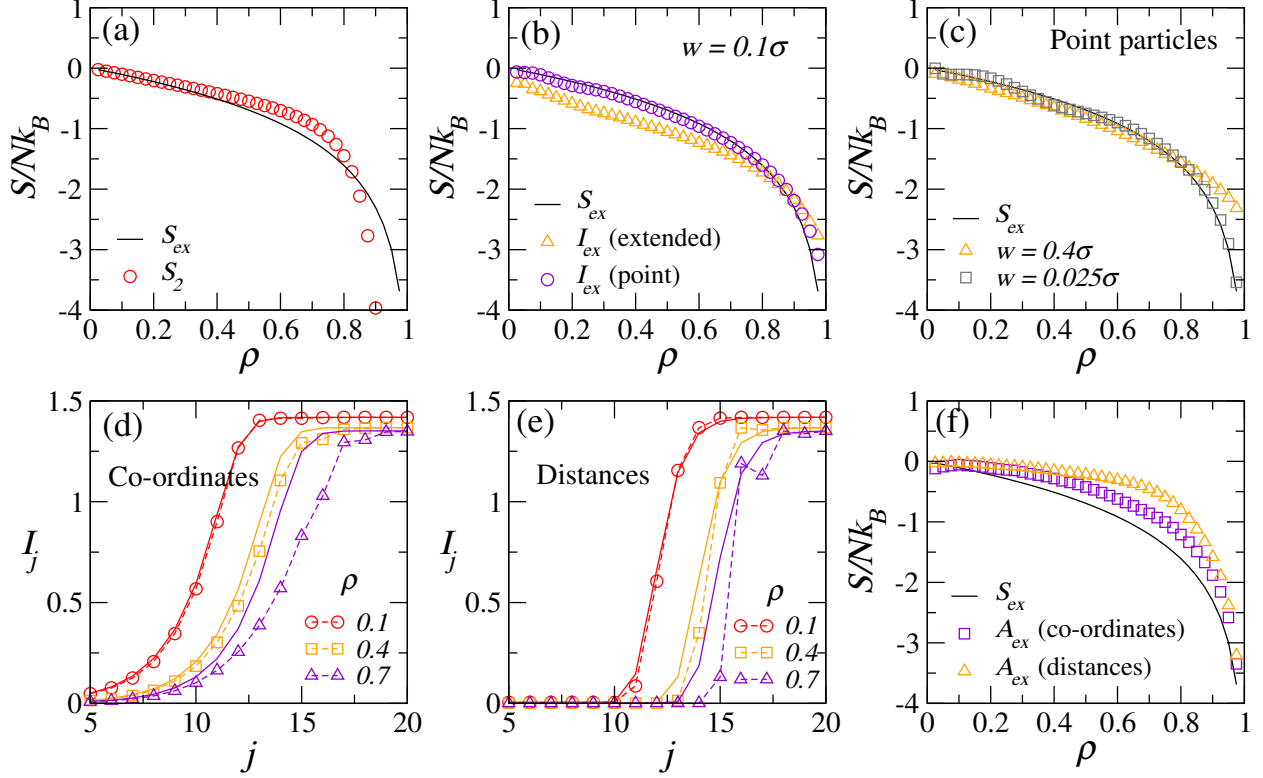


FIG. 4. Plots of various entropy estimates for the 1D hard rod gas: (a) S_2 and S_{ex} vs. ρ . (b) Comparison of grid-based CID estimates with S_{ex} . The two data sets are when the discretization is done by taking the rods to be points or extended particles. (c) Variation of CID with grid size used for discretization, for the point representation. The grid-based CID data have been scaled (not shifted) to match S_{ex} . (d) Bit-wise CID of the particle co-ordinates as a function of the bit-depth j . (e) Bit-wise CID of successive particle distances as a function of the bit-depth j . The dashed lines correspond to the hard-rod system at the given density, and the solid lines correspond to the ideal gas at the same density. (f) Excess information density A_{ex} for the bit-resolved CIDs.

dashed lines correspond to the hard-rod system at a given density, and the solid lines correspond to the ideal gas at the same density. $j = 1$ represents the most significant bit (MSB). The I_j curves exhibit the following typical behaviour: I_j starts with a low value for $j = 1$, increases gradually with j and saturates to a maximum after a certain bit depth. The maximum value of I_j corresponds to a fully random (and hence incompressible) string. Because of the sorting of the particles, the strings formed by the lower bits tends to be correlated and hence have lower CID. For the CID of the particle co-ordinates, the ideal gas has a higher information density than the hard rod gas at any density. This is to be expected

as the ideal gas particles are completely uncorrelated. This is also generally true for the CID of the particle distances. However, for $\rho \gtrsim 0.6$, the I vs. j curve shows a drop in I at $j \approx 16$. This is because the distribution of inter-particle distances get narrower with increasing density. As a result, the inter-particle distances are highly correlated, leading to a drop in the information entropy. The corresponding area difference A_{ex} is shown in Fig. 4(f). We note that even though the position-based bit-wise CID does not agree quantitatively with the thermodynamic entropy, the difference is not very large, and might be due to finite-size effects. We see that for the CID of the co-ordinates, the excess information content matches well with the excess entropy, whereas that of the inter-particle distances does not. In what follows, we will not consider the finite-particle representation for the grid-based CID or the distance-based bit-wise CID estimates.

D. Two-dimensional melting for soft-core systems

Another equilibrium system that we considered is the two-dimensional mono-disperse soft-core system exhibiting re-entrant crystallization with a maximum melting temperature T_m at density ρ_m . In this system we can separate the effect of the density and ordering on the entropy. In fact, this system undergoes a liquid-hexatic transition that, depending on density, may be either first order ($\rho < \rho_m$) or continuous (at higher densities) [27]. We consider a soft-disk model system, where pair particles interact via finite range and purely repulsive potential

$$V(r_{ij}) = \frac{\epsilon}{\alpha} (1 - r_{ij}/\sigma)^\alpha \Theta(1 - r_{ij}/\sigma) \quad (14)$$

where r_{ij} is the distance between particle i and j , and Θ denotes the Heaviside function. The potential vanishes continuously at $r_{ij} = \sigma$, where σ is the diameter of the disk. The exponent α determines the softness of the potential. Here, we choose $\alpha = 2.0$ (the “harmonic” model). ϵ and σ define our units of energy and length respectively. The maximum melting temperature T_m for the harmonic system is approximate 7.10×10^{-3} at a crossover density $\rho_m \approx 1.42$.

We consider a square simulation box of sides $L = 58\sigma$, and vary ρ by changing the number of disks N . We slowly quench the high temperature equilibrium liquid states until target temperature $T = 3.3 \times 10^{-3}$. Then we equilibrate the system at constant volume and temperature for at least 10^7 MD steps and configurations are sampled for next 10^7 MD

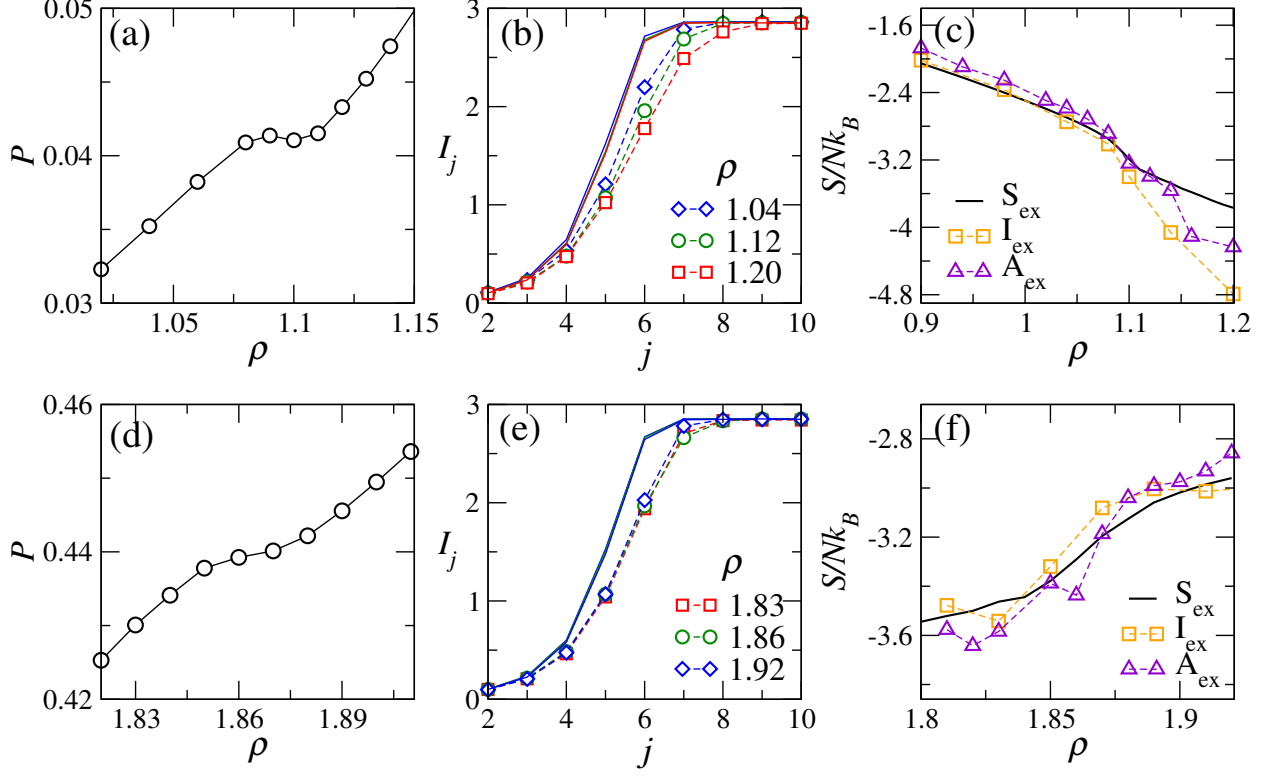


FIG. 5. The isothermal equation of states at $T = 3.3 \times 10^{-3}$ for harmonic systems in a wide range of density. (a) At low density, the equation of states shows Mayer-Wood loop. (d) At high density, the pressure increases monotonically. The compression information density as a function of bit-depth j at (b) low and (e) high densities. The dashed lines correspond to the soft-core systems at different densities, and the solid lines correspond to ideal gas systems at same densities. The rhombus-shaped symbols denote liquid states, the circles are hexatic states and the squares are solids. (c) and (f) The various excess entropy S_{ex} , I_{ex} and A_{ex} as a function of density. The curves of I_{ex} are scaled by multiplying a fitting parameter 215 and 195 respectively, and the curves of A_{ex} is scaled with fitting parameter 2.2 for (c) and (f).

steps at intervals of 10^5 MD steps. Simulations were performed both below and above ρ_m , using a parallelized version of LAMMPS [28].

In Fig 5 (a), the isothermal equation of states $P(\rho)$ shows a Mayer-Wood loop [29] at low density, suggesting first-order coexistence of the isotropic liquid and hexatic phases. By fitting the curve with a tenth-order polynomial and determining the boundaries of coexistence with a Maxwell construction, the coexistence region is found to be located in the density range $\rho=1.08$ to 1.11 . When we increase the pressure by a factor of around 10, we

find a hexatic to liquid transition at $\rho \approx 1.865$ (see Fig 5 (d)). As both the low-density and the high-density phase transitions are effectively free of hysteresis, we can compute the thermodynamic excess entropy from the equation of state by thermodynamic integration (see Fig 5 (c)(f)).

For the grid-based CID, we discretize the configuration with a square grid fine enough that no more than one disk can occupy a grid cell, resulting in a total number of cells equaling $2^9 \times 2^9$, and a bin-size of approximately $\sigma/8$. In Fig. 5 (b)(e), we plot the compression density as a function of the bit-depth j for target systems and ideal gas systems at same density with the alphabet $\alpha = \{0, 1, 2, 3\}$ indicating the combination of x and y coordinates. As expected, at lower bits the system has less information, because the box is divided into four parts and only 4 string patterns form the compressed string. For higher (less significant) bits, the compression density approaches that of a random string, indicating that, beyond these bits the coordinates provide no information on the physical state of the system. Here, we just consider the value at lower bits where the compression density is less than that of random string. For more ordered structures, the bit-depth at which the CID approaches that of the random string is higher. As a result, the value of I_j of solid states is less than that of liquid states at same bit-depth j .

In Fig. 5 (c)(f), we compare the excess entropy obtained by the three methods mentioned above. We note that the absolute value of the bit-wise CID entropy differs significantly from the thermodynamic entropy. However, the qualitative density dependence is similar. This is best seen by scaling the CID results with an adjustable fitting parameter. We stress that the fact that a scale adjustment is necessary, seriously undermines the role of the CID as a quantitative entropy estimator. Yet, we note that, after this *ad hoc* rescaling, all entropies behave qualitatively similarly, although the two CID entropies differ from the thermodynamic S_{ex} and from each other. Importantly, at higher densities, all estimates of the entropy increase with density, demonstrating that all method are more sensitive to positional correlations than to density.

E. Jamming transition for bi-disperse systems in 2D

Moving from equilibrium to non-equilibrium off-lattice models, we next consider jamming in a bi-disperse two-dimensional system. A system is said to be jammed when it develops

a yield stress [30]. Jamming transitions have been observed in a variety of systems, such as granular systems, colloids and cells [31–33]. Here we study various entropy measures for a jammed system. Such systems are not in an equilibrium state, yet are not driven either.

Here, we consider a two-dimensional equimolar binary mixture of harmonic soft disks ($\alpha = 2$ in Eq. 14) in a square box of sides $L = 150\sigma_S$, where σ_S is the width of the smaller disk, at zero temperature. The ratio of diameters of big to small disks is 1.4, so as to suppress crystallization. The systems are prepared by quenching from initially random states. Here, we use a fast inertial relaxation engine (FIRE) algorithm [34] to implement the minimization of the potential energy. Periodic boundary conditions are applied. The simulations were performed on an ensemble of 1000 harmonic systems over a wide range of volume fractions.

The configurations were discretized with a grid size approximately $\sigma_S/4.0$ and the positions of the disks are sorted using a 512×512 Hilbert scan for bit-wise CID calculation. We convert the configurations into binary strings ignoring the type of disks, *i.e.*, we only consider if a grid cell is occupied or not. Fig 6(a) shows the excess compression density I_{ex} and A_{ex} obtained from the bit-wise compression of the particle co-ordinates, as a function of the volume fraction. Both I_{ex} and A_{ex} decrease smoothly as the volume fraction increases across the jamming point $\phi_J \approx 0.84$. The curve of I_{ex} is scaled to match the values of bit-wise CID. In Fig. 6(b), we show the pair correlation entropy S_2 as a function of the packing fraction ϕ . While the first peak of $g(r)$ is supposed to diverge at the jamming point J due to the formation of contacts, when numerically computing the correlations, this divergence is not captured due to the finite width of the $g(r)$ bins. The S_2 results shown here must therefore be interpreted accordingly. We find that S_2 shows a minimum near the jamming point J . The CID measures however do not show this feature.

F. Three-dimensional Lennard Jones fluids

Little work has been done on data-compression based entropy estimates in dimensions higher than two (see, however, ref. [12]). As a test of the various entropy estimators, we study several three-dimensional systems, both in and out of equilibrium. First, we consider a three-dimensional Lennard-Jones fluid to test the generalization of bit-resolved CID in higher dimensions. We performed constant-volume and constant-temperature molecular dynamics simulations on a system of Lennard-Jones particles without shifted potential in a cubic box

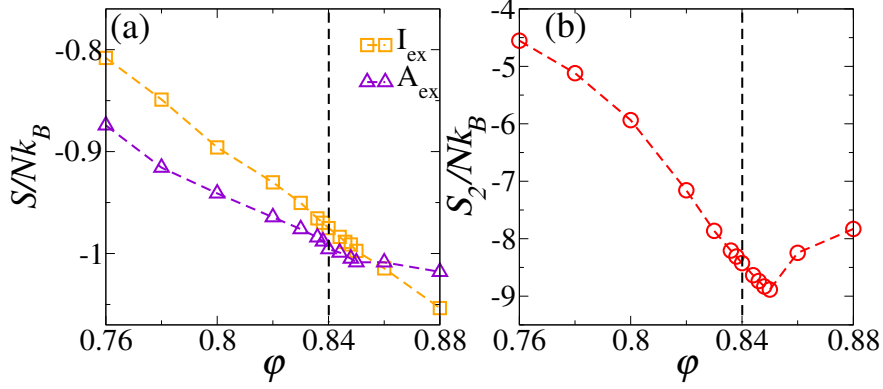


FIG. 6. The excess compression information density I_{ex} and A_{ex} decreases smoothly with volume fraction increases. The curve of excess grid based CID I_{ex} is scaled by a factor of 2.5. The dashed line indicates the location of point J. (b) Pair correlation entropy S_2 as a function of the volume fraction.

of sides $L = 29\sigma$. The potential cutoff is 4.0σ , where σ is the Lennard-Jones diameter. From the simulations, we obtain the equation of state at $T = 2.0$ in the density range from 0.1 to 0.8. The excess thermodynamic entropy calculated by thermodynamic integration is consistent with previous works as shown in Fig. 7 (b) [1, 35].

We order the coordinates of all particles in a cubic 3D system using a $128 \times 128 \times 128$ three-dimensional Hilbert scan curve. The configurations are sampled at intervals of 10^5 MD steps, giving a total of 10^3 samples starting from ten independent equilibrium liquid states. By performing bit-wise data compression on the coordinates of the particles, where the j -th bit of the x , y and z coordinates were combined into a single bit string of length N with an alphabet $\alpha = \{0, 1, \dots, 7\}$.

We also calculate the structural entropy S_2 and grid-based CID I_{ex} . Here, we discretize the configuration on a $128 \times 128 \times 128$ cubic lattice, where the grid size is small enough that only one particle occupies a grid cell. As shown in Fig. 7 (a), the differences of compressed information density of each bit between ideal gas and fluids are small, especially at low density. As shown in Fig. 7 (b), the values of I_{ex} show a large deviation from the thermodynamic excess entropy at higher densities. Similarly, the bit-wise CID A_{ex} can only be made to resemble the thermodynamic entropy scaling with an *ad hoc* factor. The inset shows the results calculated from Eq.(11) without rescaling. Clearly, the excess entropies obtained from data compression without adjustment are much smaller than the values obtained by

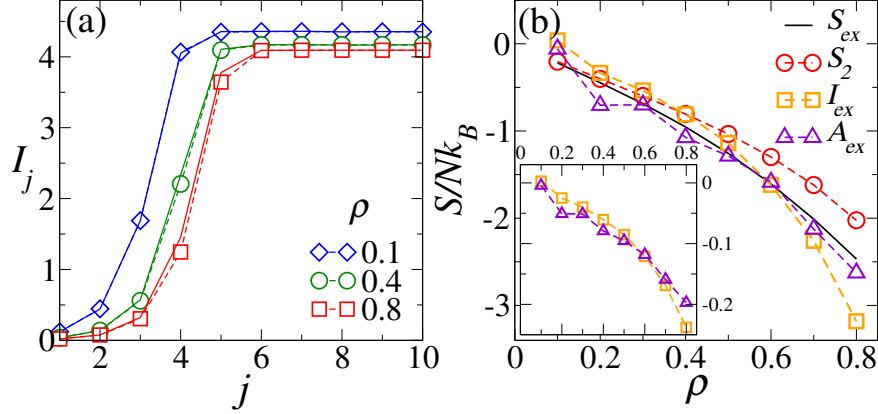


FIG. 7. (a) The CID as a function of bit-depth for three-dimensional Lennard Jones systems at various densities. The dashed curves correspond to the target system at the given density, and the solid lines denote the ideal gas at the corresponding density. (b) The various excess entropy as a function of density at $T = 2.0$. The curve of grid-based CID scaled by a factor of 8.53. The inset shows the values of I_{ex} and A_{ex} as a function of density calculated via Eq. (11).

thermodynamic integration. In fact, the difference in scale is close to two orders of magnitude. It is conceivable that part of this very large discrepancy is due to finite size effects in the value of the CID, but this is bad news too, as the finite size correction to the CID appears to converge rather slowly with system size, suggesting that the extrapolation to the thermodynamic limit (if this is indeed the significant reason for the quantitative difference) may not be feasible. Both the structural entropy S_2 , grid based I_{ex} and bit-wise A_{ex} CID decrease as density increases. Not surprisingly, the structural entropy S_2 agrees well with the total excess entropy at low densities.

We also consider the convergence rate of the bit-wise CID A_{ex} as shown in Fig.8. The convergence rate is very slow, scaling as $\log_2(\log_2 N)/\log_2 N$, as also observed by Martiniani *et al.* [11]. Due to the large error bars at smaller system sizes, we only use the 3 largest system sizes to estimate the extrapolated values. However, the uncertainty in the extrapolated values is large.

G. Cyclically Sheared Binary Lennard-Jones Mixture

Our next three-dimensional model system is a 80:20 binary mixture of Lennard-Jones particles subjected to athermal cyclic shear. The particles interact via a shifted and truncated

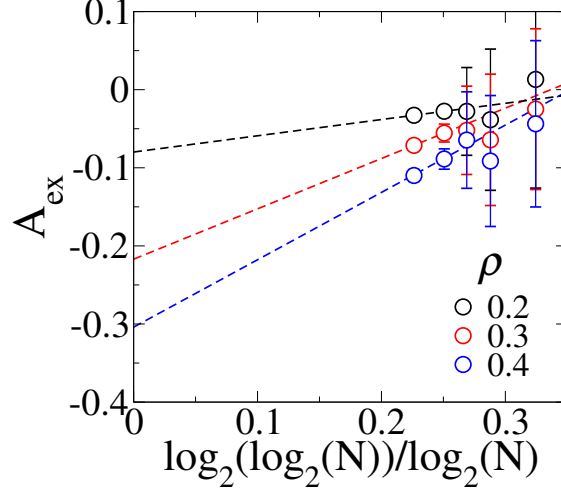


FIG. 8. The convergence of bit-wise CID for three-dimensional LJ fluids at various densities. The dashed lines are linear fits to the 3 largest system sizes.

Lennard-Jones potential:

$$U_{\alpha\beta}(r) = \begin{cases} 4\epsilon_{\alpha\beta} \left[\left(\frac{\sigma_{\alpha\beta}}{r} \right)^{12} - \left(\frac{\sigma_{\alpha\beta}}{r} \right)^6 \right] \\ \quad + 4\epsilon_{\alpha\beta} \left[c_{0\alpha\beta} + c_{2\alpha\beta} \left(\frac{r}{\sigma_{\alpha\beta}} \right)^2 \right], & r < r_{c\alpha\beta} \\ 0, & r \geq r_{c\alpha\beta} \end{cases} \quad (15)$$

where $\alpha, \beta \in \{A, B\}$ represent the particle type, $r_{c\alpha\beta} = 2.5\sigma_{\alpha\beta}$ is the cut-off distance, and the parameters $\epsilon_{AB}/\epsilon_{AA} = 1.5$, $\epsilon_{BB}/\epsilon_{AA} = 0.5$, $\sigma_{AB}/\sigma_{AA} = 0.8$, $\sigma_{BB}/\sigma_{AA} = 0.88$. The constants $c_{0\alpha\beta}$ and $c_{2\alpha\beta}$ are chosen such that the potential and the forces decay smoothly to zero at $r = r_{c\alpha\beta}$. The energy and length are in the units of ϵ_{AA} and σ_{AA} respectively.

The initial configurations are obtained from equilibrium liquid configurations by performing an energy minimization. These inherent structures are then subjected to periodic shearing, a cycle of which involves applying the strain sequence: $0 \rightarrow \gamma_{max} \rightarrow -\gamma_{max} \rightarrow 0$, for a given strain amplitude γ_{max} . The deformations are performed through an athermal quasi-static (AQS) protocol where an affine transformation of co-ordinates $x' = x + d\gamma \times z$; $y' = y$; $z' = z$ is applied with $|d\gamma| \ll 1$, followed by an energy minimization. The shearing is done until the system reaches a steady state. For small strain amplitudes, the stress is proportional to the strain and the system is characterized by localized particle rearrangements or avalanches. Above a critical strain amplitude γ_y , there is a drop in the stress as the system no longer recovers from applied stress, *i.e.*, the avalanches are system spanning.

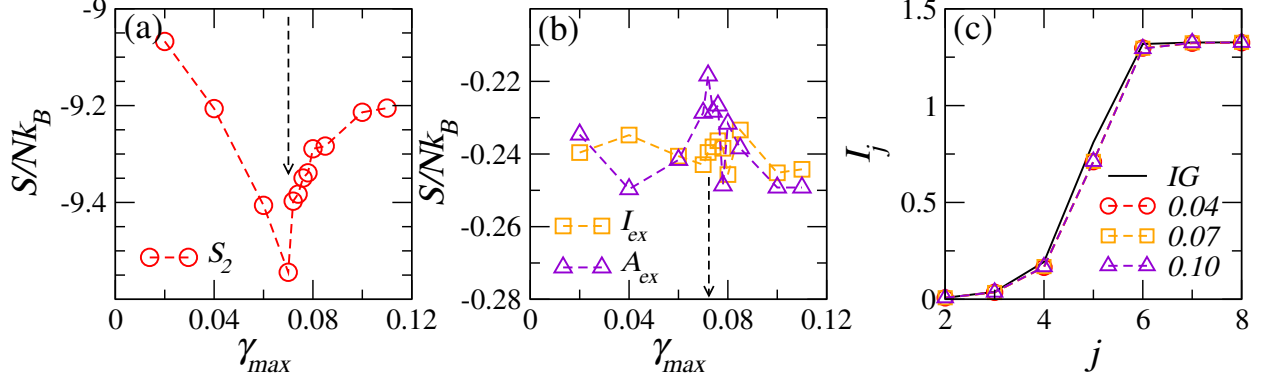


FIG. 9. (a) and (b) show S_2 , I_{ex} and A_{ex} for the cyclically sheared binary LJ system as a function of the maximum shear amplitude γ_{max} . The arrow denotes the yielding point $\gamma_y = 0.072$ [36]. (c) shows the I_j vs. j curves for different γ_{max} , and IG denotes the ideal gas reference.

This is identified as the yielding point.

In the following, we present our analysis of the simulation data of Leishangthem et al.[36], for the system size $N = 64000$ (51200 A and 12800 B particles), number density $\rho = 1.2$, and initial configurations prepared from liquid states at a reduced temperature $T = 1$. The yielding point for this system is $\gamma_y = 0.072$ [36]. In Fig. 9 (a) and (b) we show the pair correlation entropy S_2 and the CID measures for the cyclically sheared binary Lennard-Jones mixture, for various strain amplitudes. Below the yielding point, S_2 decreases with γ_{max} . At the yielding point, we observe a sharp jump in S_2 . This is in line with our expectation, as the states closer to yielding are more annealed. The CID measures however do not show any clear signal of this transition. This is yet another indication that the different measures of non-equilibrium entropy may yield very different results. In Fig. 9(c) we show I_j vs. j of the particle co-ordinates for different strains γ_{max} . As seen, the curves for the different strains do not differ much.

H. Cyclically Sheared Binary Soft-Sphere Mixture

Very similar results are obtained for an equimolar, binary mixture of soft spheres subjected to athermal cyclic shear. The interaction potential is given by the harmonic version

of the potential given in Eqn. 14

$$U_{\alpha\beta} = \begin{cases} \frac{1}{2}\epsilon \left(1 - \frac{r}{\sigma_{\alpha\beta}}\right)^2, & r < \sigma_{\alpha\beta} \\ 0, & r > \sigma_{\alpha\beta} \end{cases} \quad (16)$$

where, $\alpha, \beta \in \{A, B\}$ represent the particle type, $\epsilon = 2.0$ is the strength of the interactions, $\sigma_{\alpha\beta} = (\sigma_\alpha + \sigma_\beta)/2$, σ_α is the diameter of the α particle, and $\sigma_B/\sigma_A = 1.4$. The lengths are in units of σ_A . Depending on the packing fraction ϕ , the initial states for the shearing are prepared differently. For ϕ less than the isotropic jamming density $\phi_j = 0.648$ [37], they are obtained by compressing equilibrium hard sphere configurations at $\phi = 0.363$, through Monte Carlo simulations. For $\phi > \phi_j$, jammed configurations at ϕ_j are first obtained using the procedure described in [37]. These are then compressed up to the desired density followed by an energy minimization. The shearing is done through the AQS protocol described in the previous subsection, until a steady state is reached.

For densities below ϕ_j , the system shows three different states as a function of the strain amplitude γ_{max} . For small values of γ_{max} , the system shows point reversibility, *i.e.*, the path traced by the system in the configuration space during the backward shear is the same as that of the forward shear. At intermediate strain amplitudes, the system shows loop reversibility, *i.e.*, the system comes back to the same configuration at the end of every shear cycle. For larger strain amplitudes, the system goes to an irreversible diffusive state. For $\phi > \phi_j$, the system undergoes yielding at a critical γ_{max} , similar to the case of the binary LJ mixture. We analyse here two packing densities, $\phi = 0.627$ and 0.72 , corresponding to below and above the jamming density, the configurations for which are obtained from the simulations of Das et al. [38]. The system size is $N = 2000$ particles, and data has been averaged over 9 independent runs.

Fig. 10 shows S_2 and the various CID estimates evaluated in the steady state as a function of γ_{max} , for $\phi = 0.627$ (top panel) and $\phi = 0.72$ (bottom panel). It must be noted, however, that the $g(r)$ curves below the jamming density show a power-law divergence at $r = \sigma$ [38]. This implies that $S_2 = -\infty$ according to Eq. (5). Nevertheless, we show the results of S_2 computed using a fixed bin-width of 0.02σ for the $g(r)$ calculations. For $\phi = 0.627$, S_2 shows a dip around $\gamma_{max} \approx 0.03$ corresponding to the transition from point reversible to loop-reversible state. For $\gamma_{max} > 0.38$, the system transitions into an irreversible state, and a corresponding drop in S_2 is seen. The fluctuations in I prevent us from making any

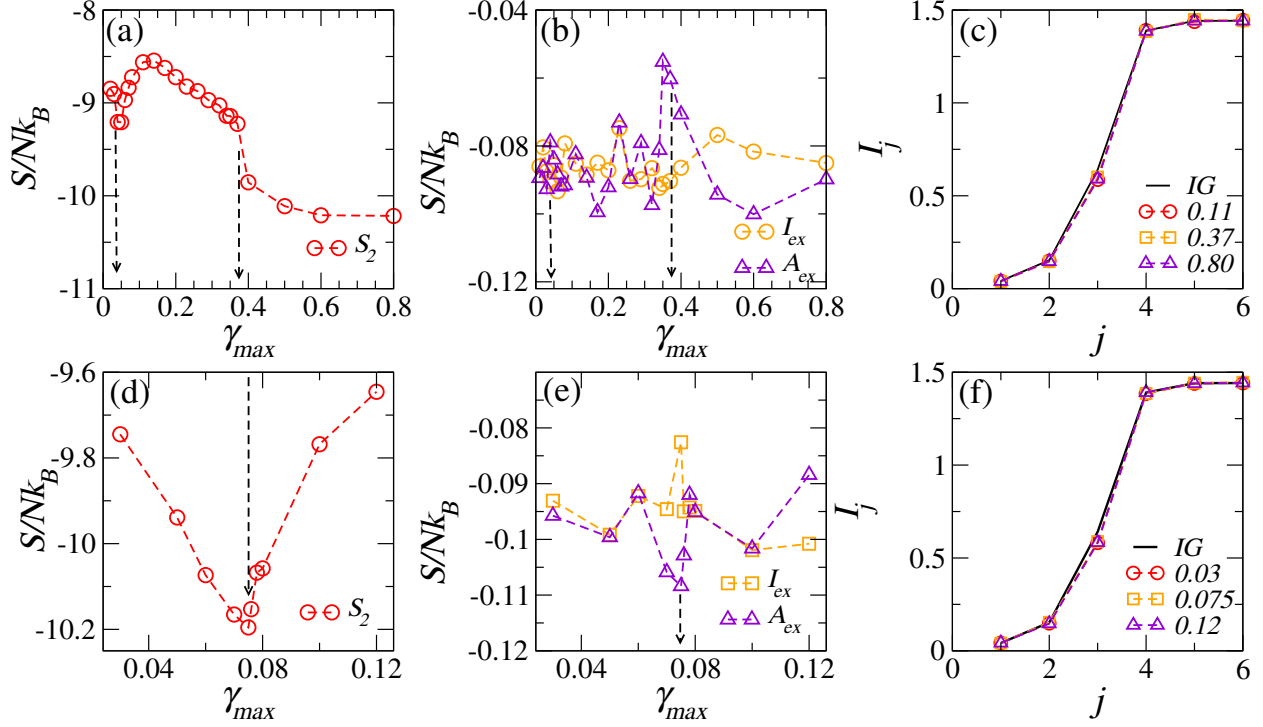


FIG. 10. S_2 and the various CID estimates for cyclically sheared soft spheres as a function of γ_{max} , for $\phi = 0.627$ (top row) and $\phi = 0.72$ (bottom row). The arrows denote the various transition points (see text). (c) and (f) show the corresponding I_j vs. j curves for various γ_{max} , and IG denotes the ideal gas reference.

statements near the absorbing transition at $\gamma_{max} = 0.03$. For $\phi = 0.72$ (bottom panel), S_2 shows a minimum corresponding to the yielding point at $\gamma_{max} = 0.075$. Again, the CID measures do not show any clear signal of this transition. Similar to the cyclically sheared binary Lennard-Jones system, the bit-wise compression curves for the soft-spheres [Figs.10(c) and (f)] do not show much variation for the different strain amplitudes.

IV. SUMMARY AND CONCLUSIONS

We have investigated the use of computational information density as a quantitative measure of the entropy of a variety of equilibrium and out-of-equilibrium systems. The performance of the methods based on data compression varies from reasonable to miserable: In the simplest off-lattice example, *viz.*, the equilibrium one-dimensional hard rod gas, the CID measures perform fairly well in capturing the entropy of the systems. This is perhaps not

surprising as the coordinates of a one-dimensional systems map naturally on a linear string, unlike higher-dimensional systems. However, for non-equilibrium systems - in particular driven systems, there is little agreement between structure-based and information based entropy estimates.

The structure based entropy, seems to capture the ordering transitions in all the cases studied. This prompts further investigation of structural correlation based entropy measures in out of equilibrium conditions. In the case of driven system, the differences in the order are very subtle and are apparently not captured by either of the information density measures studied here.

It is interesting to compare the predictions of the bit-resolved CID (A) with the grid-based version (I). A crucial difference between the computation of I and A is that when we compare I with thermodynamic or structure based entropies is that the grid-based I is only known up to a constant that is not known *a priori*, and is therefore determined by fitting. In contrast, there is no such unknown offset when we compare the parameter-free A with the thermodynamic data. Not surprisingly, in the latter case, the agreement is often less good than that for the (fitted) I .

Whilst it is not surprising that the fitted results agrees better than a procedure with no adjustable parameters, there may be other reasons why the bit-wise procedure is not in agreement with the thermodynamic data. There might, for instance, be other ways to extract an excess entropy from the bit-wise compressed data.

Also, as we discuss below, whilst the LZ data compression algorithm that we use is lossless, it does build up its “dictionary” using a finite sliding window. It is conceivable that the width of this window affects the compression results. However, we have not tested this systematically.

With these caveats in mind, we can make the following broad statements: (i) For equilibrium systems, both the grid-based and bit-wise CID measures show reasonable agreement with the thermodynamic entropy. (ii) For non-equilibrium systems, which are not driven externally, both the grid-based and bit-wise CID measures show only qualitative agreement with structure based entropy, in capturing the various non-equilibrium transitions. (iii) For non-equilibrium systems which are externally driven (cyclically sheared binary soft-sphere and binary Lennard-Jones systems in 3D), both the methods perform equally poorly, in the sense that they fail to capture the entropy changes as observed by S_2 . (iv) While there

are cases where the grid-based CID performs better than the bit-wise CID (and vice-versa), neither method is significantly better than the other, be it that I requires an arbitrary scale factor.

We also note a practical limitation of the data compression approach: the LZ77 algorithm that we use here is quite slow for long input strings, meaning that for equilibrium systems it would not be faster than other available methods for entropy calculation. While the LZ77 algorithm is supposed to converge to the Kolmogorov complexity in the thermodynamic limit, the rate of this convergence is quite slow ($\sim \log_2 \log_2 N / \log_2 N$) (see, *e.g.* [11]). This implies that the system sizes that we consider here may not be sufficiently large to observe convergence. Moreover, as we mentioned above, any practical implementation of the LZ77 algorithm (and most other compression methods) uses a sliding window – a fixed-length buffer that slides over the given symbolic string – within which it computes the LZ77 factorization. This is necessary to keep the memory requirements and the computational cost reasonable. Consequently, such an implementation while lossless, would not give the correct value of the complexity for very long strings. The effect of the finite window size may also limit the use of CID as a quantitative entropy estimator.

These considerations suggest that the CID measures studied here may, at this stage, not offer competitive approaches to estimate non-equilibrium entropies. However, the methods do offer an interesting perspective on the relation between information and entropy in physical systems. Thus we conclude that, while enticing, the use of information based entropy measures – particularly attractive in nonequilibrium contexts – requires further insights and developments to be employed as a useful tool in understanding the nature of order and entropy in equilibrium and nonequilibrium situations.

ACKNOWLEDGMENTS

The authors would like to thank in particular Stefano Martiniani for much practical help, and also Dov Levine, and Roy Beck-Barkai for useful discussions. The authors acknowledge support from UKIERI-DST under Grant No.s IND/CONT/G/16-17/104, DST/INT/UK/P-149/2016. This research was supported in part by the National Science Foundation under Grant No. NSF PHY-1748958, and the hospitality at KITP, UCSB, under the program “Memory Formation in Matter” is gratefully acknowledged by DF and SS. We also thank

the International Centre for Theoretical Sciences (ICTS) for hospitality and support during the program “Entropy, Information and Order in Soft Matter” ICTS/eiosm2018/08. SS acknowledges support through the J C Bose Fellowship (DST, India).

REFERENCES

- [1] D. Frenkel and B. Smit, *Understanding Molecular Simulation: From Algorithms to Applications*, 2nd ed. (Academic Press, New York, 2002).
- [2] N. Xu, D. Frenkel, and A. J. Liu, Phys. Rev. Lett. **106**, 245502 (2011).
- [3] D. Asenjo, F. Paillusson, and D. Frenkel, Phys. Rev. Lett. **112**, 098002 (2014).
- [4] S. Martiniani, K. J. Schrenk, J. D. Stevenson, D. J. Wales, and D. Frenkel, Phys. Rev. E **93**, 012906 (2016).
- [5] J. G. Kirkwood and E. M. Boggs, J. Chem. Phys. **10**, 394 (1942).
- [6] H. S. Green, *The Molecular Theory of Fluids* (North-Holland, Amsterdam, 1952).
- [7] R. E. Nettleton and M. S. Green, J. Chem. Phys. **29**, 1365 (1958).
- [8] H. J. Ravech, J. Chem. Phys. **55**, 2242 (1971).
- [9] D. C. Wallace, J. Chem. Phys. **87**, 2282 (1987).
- [10] A. Baranyai and D. J. Evans, Phys. Rev. A **40**, 3817 (1989).
- [11] S. Martiniani, P. M. Chaikin, and D. Levine, Phys. Rev. X **9**, 011031 (2019).
- [12] R. Avinery, M. Kornreich, and R. Beck, Phys. Rev. Lett. **123**, 178102 (2019).
- [13] O. Melchert and A. K. Hartmann, Phys. Rev. E **91**, 023306 (2015).
- [14] E. Estevez-Rams, R. Lora-Serrano, C. Nunes, and B. Aragón-Fernández, Chaos: An Interdisciplinary Journal of Nonlinear Science **25**, 123106 (2015).
- [15] N. S. Flann, H. Mohamadlou, and G. J. Podgorski, Biosystems **112**, 131 (2013).
- [16] D. J. Galas, M. Nykter, G. W. Carter, N. D. Price, and I. Shmulevich, IEEE Transactions on Information Theory **56**, 667 (2010).
- [17] V. Benci, C. Bonanno, S. Galatolo, G. Menconi, and V. M., Discrete and Continuous Dynamical Systems - B **4**, 935 (2004).
- [18] A. N. Kolmogorov, International Journal of Computer Mathematics **2**, 157 (1968).

- [19] G. J. Chaitin, J. ACM **13**, 547 (1966).
- [20] T. M. Cover and J. A. Thomas, *Elements of Information Theory* (John Wiley & Sons, Hoboken, 2006).
- [21] C. E. Shannon, The Bell System Technical Journal **27**, 379 (1948).
- [22] C. Vega, E. Sanz, J. L. F. Abascal, and E. G. Noya, J. Phys.: Cond. Mat. **20**, 153101 (2008).
- [23] J. Ziv and A. Lempel, IEEE Transactions on Information Theory **23**, 337 (1977).
- [24] A. Banerjee, M. K. Nandi, S. Sastry, and S. Maitra Bhattacharyya, J. Chem. Phys. **147**, 024504 (2017).
- [25] L. Corte, P. M. Chaikin, J. P. Gollub, and D. J. Pine, Nature Physics **4**, 420 (2008).
- [26] L. Tonks, Phys. Rev. **50**, 955 (1936).
- [27] M. Zu, J. Liu, H. Tong, and N. Xu, Phys. Rev. Lett. **117**, 085702 (2016).
- [28] See <https://lammps.sandia.gov/>.
- [29] J. E. Mayer and W. W. Wood, J. Chem. Phys. **42**, 4268 (1965).
- [30] C. S. O'Hern, L. E. Silbert, A. J. Liu, and S. R. Nagel, Phys. Rev. E **68**, 011306 (2003).
- [31] Z. Zhang, N. Xu, D. T. Chen, P. Yunker, A. M. Alsayed, K. B. Aptowicz, P. Habdas, A. J. Liu, S. R. Nagel, and A. G. Yodh, Nature **459**, 230 (2009).
- [32] D. Bi, J. Zhang, B. Chakraborty, and R. P. Behringer, Nature **480**, 355 (2011).
- [33] D. Bi, X. Yang, M. C. Marchetti, and M. L. Manning, Phys. Rev. X **6**, 021011 (2016).
- [34] E. Bitzek, P. Koskinen, F. Gähler, M. Moseler, and P. Gumbsch, Phys. Rev. Lett. **97**, 170201 (2006).
- [35] J. K. Johnson, J. A. Zollweg, and K. E. Gubbins, Molecular Physics **78**, 591 (1993).
- [36] P. Leishangthem, A. D. Parmar, and S. Sastry, Nature Communications **8**, 14653 (2017).
- [37] P. Chaudhuri, L. Berthier, and S. Sastry, Phys. Rev. Lett. **104**, 165701 (2010).
- [38] P. Das, H. A. Vinutha, and S. Sastry, arXiv:1907.08503 (2019).